

Critical phenomena in dynamical scalarization of charged black hole

Cheng-Yong Zhang,^{1,*} Qian Chen,^{2,†} Yunqi Liu,^{3,‡} Wen-Kun Luo,^{1,§} Yu Tian,^{2,4,¶} and Bin Wang^{3,5,**}

¹*Department of Physics and Siyuan Laboratory, Jinan University, Guangzhou 510632, China*

²*School of Physical Sciences, University of Chinese Academy of Sciences, Beijing 100049, China*

³*Center for Gravitation and Cosmology, College of Physical Science and Technology, Yangzhou University, Yangzhou 225009, China*

⁴*Institute of Theoretical Physics, Chinese Academy of Sciences, Beijing 100190, China*

⁵*Shanghai Frontier Science Center for Gravitational Wave Detection, Shanghai Jiao Tong University, Shanghai 200240, China*

We report a new black hole (BH) scalarization mechanism and disclose novel dynamical critical phenomena in the process of the nonlinear accretion of the scalar field into BHs. The accretion process can transform a seed BH into a final scalarized or bald BH, depending on the initial parameter of the scalar field p . There is a critical parameter p_* and near it all intermediate solutions are attracted to a critical solution (CS) and stay there for a time scaling as $T \propto -\gamma \ln |p - p_*|$. At late times, the solutions evolve into scalarized black holes (BHs) if $p > p_*$, or bald BHs if $p < p_*$. The final masses of the resulting scalarized/bald BHs satisfy power-laws $M_p - M_{\pm} \propto |p - p_*|^{\gamma_{\pm}}$ where M_{\pm} are the masses of the scalarized/bald BHs when $p \rightarrow p_*$ from above/below, and γ_{\pm} the corresponding exponents.

I. INTRODUCTION

One of the most intriguing phenomena in BH physics is the critical behavior in gravitational collapse, which has highlighted the nonlinear dynamics at the threshold of BH formation [1]. Choptuik first observed in the study of a massless scalar field collapse that there is generally a critical parameter value p_* which signals the onset of BH formation for each family of initial data parameterized by p . In the subcritical regime ($p < p_*$), the scalar field disperses to infinity, leaving a flat spacetime behind. However in the supercritical regime ($p > p_*$), a BH forms with mass satisfying the power-law $M \propto (p - p_*)^{\gamma}$ in which γ is a universal exponent. The imploding scalar wave induces a phase transition between the flat/black-hole spacetimes. The BH turns on with an infinitesimal mass for the type II transition, where the CS at the threshold is self-similar and universal [2–7]. For the type I transition in some theories, the BH turns on with a finite mass near the threshold, but does not follow the power-law. Instead, the intermediate evolutions stay near the CS with a time scaling as $T \propto -\gamma \ln |p - p_*|$. The universal CS is stationary or time-periodic [8–13]. For a detailed review, please refer to [14].

The critical behaviors reported were found between the no-black-hole/black-hole transition. In this work, we introduce novel dynamical critical phenomena during the nonlinear simulation of the bald/scalarized BH transition in theories with nonminimal coupling between the scalar and a source term. The scalarized BH can be formed by accretion of the scalar field surrounding a seed BH at the center. For the initial scalar data parameterized by p , there is a threshold p_* at where a metastable scalarized critical BH solution lives. Near the threshold, all the intermediate solutions are attracted to this CS and stay there for a time scaling as $T \propto -\gamma \ln |p - p_*|$. At late times, the intermediate solutions decay to bald BHs if $p < p_*$, or to scalarized BHs if $p > p_*$. The final values of the scalar and BH mass are discontinuous across the critical point. Thus the critical scalarization is a kind of first-order phase

transition. But unlike the case in type I critical gravitational collapse, we find that final masses of the scalarized/bald BHs follow the power-law $M_p - M_{\pm} \propto |p - p_*|^{\gamma_{\pm}}$ in which M_{\pm} are the masses of the scalarized/bald BHs when $p \rightarrow p_*$ from above/below, and γ_{\pm} the corresponding exponents.

The nonlinear accretion of the scalar field introduces a new mechanism for the BH scalarization, which is different from the spontaneous scalarization triggered by the linear tachyonic instability of the scalar field in bald BH background. Either the bald or scalarized BH is linearly stable at the same point in the model parameter space, and no intermediate attractor appears in the dynamical simulation for the spontaneous scalarization [15]. However, the new scalarization we uncovered reflects the consequences of nonlinearity. The CS behaves as an attractor, and both the final bald and scalarized BHs are linearly stable at the same point in the model parameter space.

The specific action we consider is

$$S = \frac{1}{16\pi} \int d^4x \sqrt{-g} [R - 2\nabla_{\mu}\phi\nabla^{\mu}\phi - f(\phi)I], \quad (1)$$

where R is the Ricci scalar for the metric $g_{\mu\nu}$. The real scalar field ϕ couples to a source term I through function $f(\phi)$. It is known as the Einstein-Maxwell-scalar (EMS) theory if $I = F_{\mu\nu}F^{\mu\nu}$, or the Einstein-scalar-Gauss-Bonnet (EsGB) theory if $I = R^2 - 4R_{\mu\nu}R^{\mu\nu} + R_{\mu\nu\rho\sigma}R^{\mu\nu\rho\sigma}$. These theories have attracted many attentions due to the spontaneous scalarization [16–23]. To obtain a theory allowing the bald solution, there should be $\frac{df}{d\phi}(0) = 0$. The spontaneous scalarization occurs if $\frac{d^2f}{d\phi^2}(0) > 0$ for EMS theory, or $\frac{d^2f}{d\phi^2}(0) < 0$ for EsGB theory, due to the fact that the effective mass squared of the scalar perturbation is negative, and the tachyonic instability of the bald BH is triggered. Here we focus on the EMS theory with coupling function $f(\phi) = e^{\beta\phi^4}$, in which β is a parameter. This model allows the bald solution, but the spontaneous scalarization is quenched since $\frac{d^2f}{d\phi^2}(0) = 0$. In other words, the bald Reissner-Nordström (RN) BH in this theory is linearly stable under small perturbation. But we find

it is nonlinearly unstable under large disturbance and evolves into a scalarized BH. We confirm that the EMS theories with other coupling functions such as $f(\phi) = e^{\beta\phi^n}$, $1 + \beta\phi^n$ with $n = 3, 4, 5, 6$ also have the nonlinear instability and the critical phenomena in dynamical scalarization.

II. NUMERICAL SETUP

We study the nonlinear dynamics of the spherically symmetrical BHs under large disturbance in EMS theory by adopting the Painlevé-Gullstrand-like coordinates ansatz

$$ds^2 = -(1 - \zeta^2)\alpha^2 dt^2 + 2\zeta\alpha dt dr + dr^2 + r^2 d\Omega_2^2. \quad (2)$$

Here $d\Omega_2^2$ is the line element of unit sphere S^2 and α, ζ are metric functions of (t, r) . This coordinate system is regular on the apparent horizon which locates at $\zeta = 1$. For a bald RN BH, $\alpha = 1$ and $\zeta = \sqrt{\frac{2M}{r} - \frac{Q^2}{r^2}}$.

Taking the gauge potential as $A_\mu dx^\mu = A(t, r)dt$, the Maxwell equations give

$$\partial_r A = \frac{Q\alpha}{r^2 f(\phi)}, \quad (3)$$

in which Q is the electric charge parameter. For scalarized solutions, the coupling between scalar and electromagnetic field can modulate electromagnetic energy and transform it into the scalar. Introducing auxiliary variables $\Phi = \partial_r \phi$ and $\Pi = \frac{1}{\alpha} \partial_t \phi - \zeta \Phi$, the Einstein equations give

$$\partial_r \zeta = \frac{r}{2\zeta} \left(\Phi^2 + \Pi^2 + \frac{Q^2}{r^4 f} \right) - \frac{\zeta}{2r} + r\Pi\Phi, \quad (4)$$

$$\partial_r \alpha = -\frac{r\Pi\Phi\alpha}{\zeta}, \quad (5)$$

$$\partial_t \zeta = \frac{r\alpha}{\zeta} (\Pi + \Phi\zeta) (\Pi\zeta + \Phi). \quad (6)$$

The scalar equations can be written as

$$\partial_t \phi = \alpha (\Pi + \Phi\zeta), \quad (7)$$

$$\partial_t \Pi = \frac{\partial_r [(\Pi\zeta + \Phi)\alpha r^2]}{r^2} - \frac{\alpha Q^2}{2r^4} \frac{df}{d\phi}. \quad (8)$$

Given initial ϕ and Π , we can get the initial Φ and then ζ, α from constraints (4, 5). The ζ, ϕ, Π on next time slices can be obtained from the evolution equations (6, 7, 8). The constraint (4) is used only once at the beginning.

At spatial infinity, the matter functions ϕ, Π, Φ should be zero. Then $\zeta \rightarrow \sqrt{\frac{2M}{r}}$ as $r \rightarrow \infty$. Here the constant M is the total Misner-Sharp mass of the spacetime. We introduce $s = \sqrt{r}\zeta$ to replace ζ in the simulation and set the boundary conditions for s, α as

$$s|_{r \rightarrow \infty} = \sqrt{2M}, \quad \alpha|_{r \rightarrow \infty} = 1. \quad (9)$$

The second equality implies that the coordinate time t equals the proper time at the infinity. The computational domain

ranges in (r_0, ∞) where r_0 is a bit smaller than the initial apparent horizon. We use the fourth-order finite difference method in the radial direction by compactification $z = \frac{r}{r+M}$ and discretizing z uniformly with about $2^{11} \sim 2^{12}$ grid points. The resolution is limited in the far region at late times. But it is accurate enough since we focus on the near horizon behavior. The time evolution is solved with the fourth-order Runge-Kutta method. The Kreiss-Oliger dissipation is employed to stabilize the simulation. At the first step, the constraint (4) is solved by the Newton-Raphson method [24].

We use the following families of initial data $\phi = ae^{-\left(\frac{r-cM}{wM}\right)^2}$, $\Pi = 0$. Here a, c, w parameterize the initial amplitude, center, and width of the Gaussian wave, respectively. Other types of initial data such as $\phi = a\left(1 - \tanh \frac{r}{wM}\right)$, $\Pi = 0$ are also employed. If the initial scalar locates far away from the center, one gets an initial RN BH at the center. If the initial scalar locates near the center, one gets an initial non-equilibrium charged BH, which deviates from the RN BH. For all these initial data families, we observe qualitatively the same results. We check the accuracy and convergence of our numerical method in various ways and find that it converges to the fourth-order.

III. NUMERICAL RESULTS

We fix $M = 1$, $Q/M = 0.9$ and $\beta = 200$ to present our results. In Fig.1, we show the evolution of the BH irreducible mass $M_h = \sqrt{\frac{A}{4\pi}} = r_h$ and the scalar value ϕ_h on the apparent horizon. A and r_h denote the area and areal radius of the apparent horizon, respectively. For initial data parameterized by p (which could be a, c or w here), there is a threshold p_* . When p is close to p_* , after a violent change at the very early times dominated by the initial data, all the intermediate solutions are attracted to a CS and stay there for a long time. By fine-tuning p to the exact critical value p_* , the evolution would stay on this CS forever, in principle. The CS corresponds to a metastable scalarized BH solution of the theory. At late times, the intermediate solutions decay to bald RN BHs if $p < p_*$, or to scalarized charged BHs if $p > p_*$. Note that the BH's irreducible mass never decreases with time, satisfying the requirement of the second law. The scalar field displays damped oscillation at the late times, indicating that the final solutions in supercritical or subcritical cases approach linearly stable scalarized or bald BHs, respectively. If p is far way from p_* , instead of being attracted to the CS, the evolution converges directly to the final state.

To understand the plateaus in Fig.1 more clearly, we calculate $\ln \left| \frac{d\phi_h}{dt} \right|$ and show the results in Fig.2. It is obvious that the nonlinear evolution can be divided into six stages. At the first stage, the solutions are closely related to the initial data. At the second stage, all the solutions display damped oscillation with damping rate $\nu_\phi \approx -0.13$. At the third stage, we get the intermediate solutions that are very close to the critical solution. The scalar fields change with

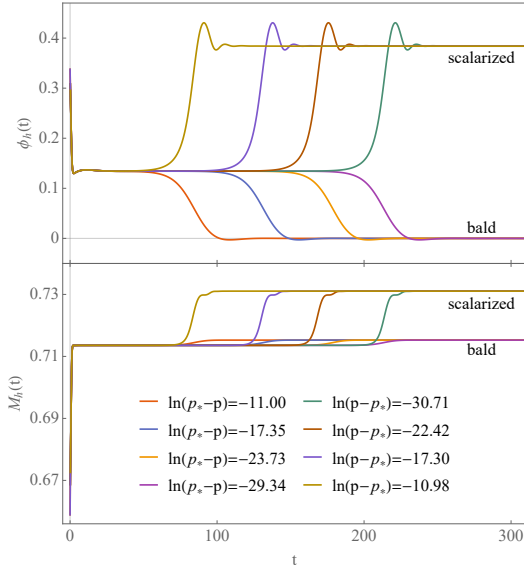


FIG. 1. The evolution of ϕ_h (upper) and M_h (lower) for various p when $Q/M = 0.9$ and $\beta = 200$. We show the results obtained from initial data family $\phi = 0.5e^{-\frac{r}{pM}}^2$. The critical value $p_* \approx 2.116895853824$. Other initial data families lead to qualitatively the same behaviors.

$|\frac{d\phi_h}{dt}| \propto e^{-0.024t}$. At the fourth stage, the solutions depart from the CS with $|\frac{d\phi_h}{dt}| \propto e^{\eta_\phi t}$ in which $\eta_\phi \approx 0.13$ for all p . At the fifth stage, the system settles down, resembling the quasinormal modes. The imaginary part of the dominate mode can be fitted as $\omega_{\phi I} \approx -0.18$ for the supercritical cases or $\omega_{\phi I} \approx -0.11$ for the subcritical cases. The sixth stage is the late-time tail with $\phi_h \propto t^{-3}$ for both the supercritical and subcritical cases.

It is clear that the intermediate plateaus in Fig.1 consist of the second, third and most part of the fourth stages displayed in Fig.2. They are intermediate solutions $\phi_p(t, r)$ corresponding to p that can be well approximated by

$$\phi_p(t, r) \approx \phi_*(r) + (p - p_*)e^{\eta_\phi t} \delta\phi(r) + \text{stable modes}. \quad (10)$$

Here $\phi_*(r)$ stands for the critical solution, $\delta\phi(r)$ is the only unstable eigenmode associated with the eigenvalue η_ϕ , analogues to the cases in type I critical gravitational collapse [4, 5, 10]. At the second and third stages, the stable modes of ϕ_p dominate. But the unstable mode dominates in the fourth stage and grows to a finite size with time T satisfying $|p - p_*|e^{\eta_\phi T} \sim O(1)$. For $t > T$ (the fifth and sixth stages), the solutions will be approximated by the end states instead of the CS. So T is the time of intermediate solution stays near the CS. It scales as $T \propto -\gamma \ln |p - p_*|$ in which $\gamma = \eta_\phi^{-1} \approx 7.4$ for both subcritical and supercritical cases. This is shown in the upper panel of Fig.3.

We further show the evolution of $\ln \frac{dM_h}{dt}$ in Fig.2 which can also be divided into six stages. There is an interesting relation:

$$\ln \frac{dM_h}{dt} \propto 2 \ln \left| \frac{d\phi_h}{dt} \right|, \quad (11)$$

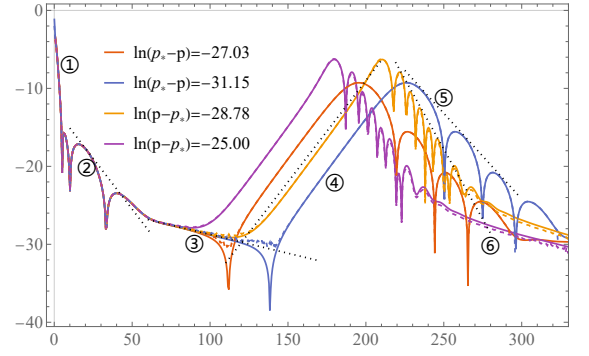


FIG. 2. The evolution of $1.2 + 2 \ln \left| \frac{d\phi_h}{dt} \right|$ (solid) and $\ln \frac{dM_h}{dt}$ (dashed) for various p when $Q/M = 0.9$ and $\beta = 200$. Both the evolutions can be divided into six stages, as labelled in the figure. Note that the evolution of $\ln \frac{dM_h}{dt}$ overlaps with that of $1.2 + 2 \ln \left| \frac{d\phi_h}{dt} \right|$ for almost all the stages. The dotted lines are the fitting curves for each stage.

for almost all stages. It holds not only for evolution with $p \simeq p_*$, but also for all initial data in our studies. This result confirm the rough relations found in [15, 25, 26]. The irreducible mass equals the BH horizon areal radius which locates at $\zeta(t, r_h) = 1$. So $\frac{dr_h}{dt} = -\frac{\partial_t \zeta}{\partial_r \zeta} |_{r_h}$. Combining (4, 6), there is $\delta r_h \sim O(\delta\phi^2)$ on the horizon for stationary solutions such as the critical or the final scalarized/bald solutions. Since the second, third and fourth stages are close to the CS, and the fifth, sixth stages are close to the final scalarized/bald BHs, (11) is expected to hold in these stages. But (11) holds even in the first stage which is highly nonlinear, so it is a rather nontrivial relation.

In the lower panel of Fig.3, we observe power-laws for the scalarized and bald BH solutions at late times:

$$M_p - M_\pm \propto |p - p_*|^{\gamma_\pm}. \quad (12)$$

Here M_p, M_\pm are the irreducible masses of the final BHs for initial data with parameters p and $p_\pm \rightarrow p_*$ from above/below, respectively. Numerically, p_* is accurate up to 10^{-12} due to the numerical accuracy limitation and we take $p_\pm = p_* \pm 10^{-12}$. The indexes $\gamma_+ \approx \gamma_- \approx 0.18$. The differences $M_p - M_\pm$ result from the scalar escaping to the infinity during the evolution. The relation (12) is absent in type I gravitational collapse. Further, the indexes γ_\pm here are related to the families of the initial data. For example, when the initial scalar locates far away from the center, more scalar will escape to the infinity, resulting in different critical and final scalarized/bald solutions from those obtained by the initial scalar locating at the center. Nevertheless, we observe the power-laws for each family of the initial data. The critical indexes also depend on the coupling function [11]. These relations need more quantitative investigation in the future.

To understand the evolution of the CS at late times and the linear stability of the final scalarized/bald BHs, we analyze the radial perturbations for the critical and supercritical/subcritical solutions. Making a coordinate transformation $dt_s = dt - \zeta dr_*$ in which $dr_* = \frac{1}{(1-\zeta^2)\alpha} dr$,

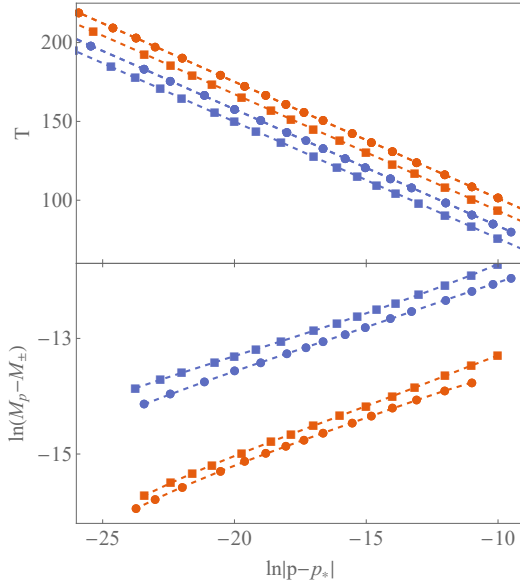


FIG. 3. Upper panel: The time T of the intermediate solution that stays near the CS with respect to $\ln|p - p_*$ when $Q/M = 0.9$ and $\beta = 200$. The lines with circle and square markers are obtained with initial conditions $\phi = 0.5e^{-(\frac{r}{pM})^2}$ and $\phi = p(1 - \tanh(\frac{r}{2M}))$, respectively. The red lines are for $p < p_*$ and the blue lines for $p > p_*$. Here all lines have $\gamma \approx 7.4$. We use the time containing the first to the fourth stage as T , which can be get easily by counting the time when ϕ_h is maximum for $p > p_*$ or minimum for $p < p_*$, as shown in Fig.1. Since the first stage takes almost the same time for different p , the coefficient γ will not be affected. Lower panel: The power-law relations $M_p - M_{\pm} \propto |p - p_*|^{\gamma_{\pm}}$ for $p < p_*$ (red) and $p > p_*$ (blue) for the two families of initial data.

supposing ϕ is the background scalar and $\delta\phi = e^{-i\omega t_s} \frac{R(r)}{r}$ is the perturbation, we get a Schrödinger-like equation [27]

$$0 = (\partial_{r_*}^2 + \omega^2 - V_{\text{eff}}) R. \quad (13)$$

Here the effective potential $V_{\text{eff}} = \frac{(1-\zeta^2)\alpha^2}{r^2} [\zeta^2 - 2r^2\phi'^2 - \frac{Q^2}{r^2 f} (1 - 2r^2\phi'^2 + \frac{2r\phi' \dot{f}}{f} + \frac{f\dot{f} - \dot{f}^2}{2f^2})]$ in which $\phi' = \partial_r \phi$ and $\dot{f} = \frac{df}{d\phi}$. The distributions of the metric functions, the background ϕ and V_{eff} for the critical and bald/scalarized solutions are shown in Fig.4. Only for the CS, there is $\int_{-\infty}^{\infty} V_{\text{eff}} dr_* < 0$ so that the CS cannot be stable [28]. Actually, the scalar perturbation has a negative effective mass squared near the horizon. So the CS has tachyonic instability, which gives precisely the unstable mode in $\phi_p(t, r)$ and drives the system away from $\phi_*(r)$. As implied in (10), if $p < p_*$, the scalar surrounding the critical BH decreases to zero by falling into the BH, except a part of the scalar field disperses to the infinity, resulting in a final RN BH. For $p > p_*$, the coupling function $f(\phi)$ plays the role of transforming the electromagnetic energy into the scalar field. The accretion of the energetic scalar field results in significant growth of the BH mass. On the other hand, the final scalar field has an effective potential barrier to balance the gravity such that it survives out of the horizon.

Using the first order WKB method for the CS, we can get

the dominant mode of the second stage $\omega \approx 0.19 - 0.13i$. The dominant modes of the fifth stage are $\omega \approx 0.61 - 0.18i$ and $\omega \approx 0.20 - 0.097i$ for the final scalarized/bald BHs, respectively. Note that all the imaginary part results from the linear analysis are consistent with nonlinear numerical fitting results within the error tolerance.

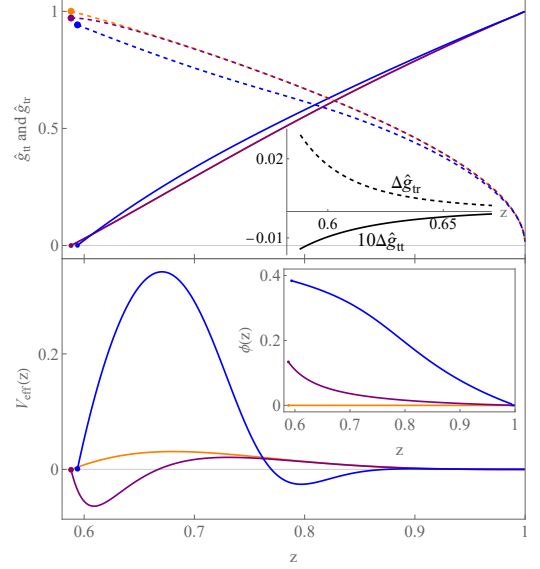


FIG. 4. Radial profiles of the metric functions $\hat{g}_{tt} = (1 - \zeta^2)\alpha^2$ (solid), $\hat{g}_{tr} = \zeta\alpha$ (dashed) and V_{eff}, ϕ for bald (orange), scalarized (blue) and critical (purple) solutions. The upper inset shows the tiny difference between the metric functions of the bald and critical solutions. Here $Q/M = 0.9$ and $\beta = 200$. The horizons of the critical and bald/scalarized solutions locate at $z \approx 0.5880, 0.5886, 0.5938$, respectively.

IV. SUMMARY AND DISCUSSION

We have found a new BH scalarization mechanism through the nonlinear accretion of the scalar field in EMS theories. This mechanism is different from the previously disclosed spontaneous scalarization triggered by the linear tachyonic instability of the bald BH, in which either the bald or scalarized BH can stay stable at the same model parameter space point. We uncover a new family of critical solutions, which separate solutions containing scalarized BHs from those containing bald BHs. In particular, we have found the dynamical critical phenomena in the bald/scalarized BH phase transition, which is analogous to those observed in type I critical gravitational collapse. The discovery of this new critical behavior has revealed interesting nonlinear dynamics at the threshold of black hole scalarization and opened up a fascinating area of research in generalized theories of relativity and in the properties of spacetimes.

ACKNOWLEDGMENTS

We thank Peng-Cheng Li, Peng Liu, Chao Niu, Xiao-Ning Wu, and Hongbao Zhang for helpful discussions. This research is supported by National Key R&D Program of China under Grant No.2020YFC2201400, and the Natural Science Foundation of China under Grant Nos. 11975235, 12005077 and 12035016, and Guangdong Basic and Applied Basic Research Foundation under Grant No. 2021A1515012374. The work of B. W. was partially supported by NNSFC under grant 12075202.

* zhangcy@email.jnu.edu.cn

† chenqian192@mails.ucas.ac.cn

‡ yunqiliu@yzu.edu.cn (corresponding author)

§ luowk@stu2020.jnu.edu.cn

¶ ytian@ucas.ac.cn

** wang_b@sztu.edu.cn (corresponding author)

- [1] M. W. Choptuik, “Universality and scaling in gravitational collapse of a massless scalar field,” *Phys. Rev. Lett.* **70** (1993), 9-12
- [2] D. Garfinkle and G. C. Duncan, “Scaling of curvature in subcritical gravitational collapse,” *Phys. Rev. D* **58** (1998), 064024 [arXiv:gr-qc/9802061 [gr-qc]].
- [3] A. M. Abrahams and C. R. Evans, “Critical behavior and scaling in vacuum axisymmetric gravitational collapse,” *Phys. Rev. Lett.* **70** (1993), 2980-2983.
- [4] C. R. Evans and J. S. Coleman, “Observation of critical phenomena and selfsimilarity in the gravitational collapse of radiation fluid,” *Phys. Rev. Lett.* **72** (1994), 1782-1785. [arXiv:gr-qc/9402041 [gr-qc]].
- [5] T. Koike, T. Hara and S. Adachi, “Critical behavior in gravitational collapse of radiation fluid: A Renormalization group (linear perturbation) analysis,” *Phys. Rev. Lett.* **74** (1995), 5170-5173 [arXiv:gr-qc/9503007 [gr-qc]].
- [6] C. Gundlach, “The Choptuik space-time as an eigenvalue problem,” *Phys. Rev. Lett.* **75** (1995), 3214-3217. [arXiv:gr-qc/9507054 [gr-qc]].
- [7] M. W. Choptuik, E. W. Hirschmann, S. L. Liebling and F. Pretorius, “Critical collapse of a complex scalar field with angular momentum,” *Phys. Rev. Lett.* **93** (2004), 131101 [arXiv:gr-qc/0405101 [gr-qc]].
- [8] R. Bartnik and J. McKinnon, “Particle-Like Solutions of the Einstein Yang-Mills Equations,” *Phys. Rev. Lett.* **61** (1988), 141-144.
- [9] E. Seidel and W. M. Suen, “Oscillating soliton stars,” *Phys. Rev. Lett.* **66** (1991), 1659-1662.
- [10] P. Bizon and T. Chmaj, “Critical collapse of Skyrmions,” *Phys. Rev. D* **58** (1998), 041501(R) [arXiv:gr-qc/9801012 [gr-qc]].
- [11] S. L. Liebling and M. W. Choptuik, “BH criticality in the Brans-Dicke model,” *Phys. Rev. Lett.* **77** (1996), 1424-1427 [arXiv:gr-qc/9606057 [gr-qc]].
- [12] M. W. Choptuik, T. Chmaj and P. Bizon, “Critical behavior in gravitational collapse of a Yang-Mills field,” *Phys. Rev. Lett.* **77** (1996), 424-427 [arXiv:gr-qc/9603051 [gr-qc]].
- [13] P. R. Brady, C. M. Chambers and S. M. C. V. Gonçalves, “Phases of massive scalar field collapse,” *Phys. Rev. D* **56** (1997), R6057-R6061 [arXiv:gr-qc/9709014 [gr-qc]].
- [14] C. Gundlach and J. M. Martin-Garcia, “Critical phenomena in gravitational collapse,” *Living Rev. Rel.* **10** (2007), 5 [arXiv:0711.4620 [gr-qc]].
- [15] C. Y. Zhang, P. Liu, Y. Q. Liu, C. Niu and B. Wang, “Dynamical charged black hole spontaneous scalarization in anti-de Sitter spacetimes,” *Phys. Rev. D* **104** (2021) no.8, 084089 [arXiv:2103.13599 [gr-qc]].
- [16] D. D. Doneva and S. S. Yazadjiev, “New Gauss-Bonnet Black Holes with Curvature-Induced Scalarization in Extended Scalar-Tensor Theories,” *Phys. Rev. Lett.* **120**, no.13, 131103 (2018) [arXiv:1711.01187 [gr-qc]].
- [17] H. O. Silva, J. Sakstein, L. Gualtieri, T. P. Sotiriou and E. Berti, “Spontaneous scalarization of black holes and compact stars from a Gauss-Bonnet coupling,” *Phys. Rev. Lett.* **120**, no.13, 131104 (2018) [arXiv:1711.02080 [gr-qc]].
- [18] G. Antoniou, A. Bakopoulos and P. Kanti, “Evasion of No-Hair Theorems and Novel Black-Hole Solutions in Gauss-Bonnet Theories,” *Phys. Rev. Lett.* **120**, no.13, 131102 (2018) [arXiv:1711.03390 [hep-th]].
- [19] P. V. Cunha, C. A. Herdeiro and E. Radu, “Spontaneously Scalarized Kerr Black Holes in Extended Scalar-Tensor-Gauss-Bonnet Gravity,” *Phys. Rev. Lett.* **123**, no.1, 011101 (2019) [arXiv:1904.09997]. [gr-qc]
- [20] A. Dima, E. Barausse, N. Franchini and T. P. Sotiriou, “Spin-induced black hole spontaneous scalarization,” *Phys. Rev. Lett.* **125** (2020) no.23, 231101. [arXiv:2006.03095 [gr-qc]].
- [21] C. A. R. Herdeiro, E. Radu, H. O. Silva, T. P. Sotiriou and N. Yunes, “Spin-induced scalarized black holes,” *Phys.Rev.Lett.* **126** (2021), 011103. [arXiv:2009.03904 [gr-qc]].
- [22] E. Berti, L. G. Collodel, B. Kleihaus and J. Kunz, “Spin-induced black-hole scalarization in Einstein-scalar-Gauss-Bonnet theory,” *Phys.Rev.Lett.* **126** (2021), 011104. [arXiv:2009.03905 [gr-qc]].
- [23] C. A. R. Herdeiro, E. Radu, N. Sanchis-Gual and J. A. Font, “Spontaneous Scalarization of Charged Black Holes,” *Phys. Rev. Lett.* **121**, no. 10, 101102 (2018). [arXiv:1806.05190].
- [24] Ó. J. C. Dias, J. E. Santos and B. Way, “Numerical Methods for Finding Stationary Gravitational Solutions,” *Class. Quant. Grav.* **33**, no.13, 133001 (2016) [arXiv:1510.02804 [hep-th]].
- [25] C. Y. Zhang, P. Liu, Y. Liu, C. Niu and B. Wang, “Evolution of Anti-de Sitter black holes in Einstein-Maxwell-dilaton theory,” [arXiv:2104.07281 [gr-qc]].
- [26] C. Y. Zhang, P. Liu, Y. Liu, C. Niu and B. Wang, “Dynamical scalarization in Einstein-Maxwell-dilaton theory,” [arXiv:2111.10744 [gr-qc]].
- [27] P. G. S. Fernandes, C. A. R. Herdeiro, A. M. Pombo, E. Radu and N. Sanchis-Gual, “Spontaneous Scalarisation of Charged Black Holes: Coupling Dependence and Dynamical Features,” *Class. Quant. Grav.* **36** (2019) no.13, 134002. [arXiv:1902.05079].
- [28] W.F. Buell and B.A. Shadwick, “Potentials and bound states,” *Am. J. Phys.* **63** (1995) 256.